Original article

Institution of MECHANICAL ENGINEERS

Journal of MATERIALS: DESIGN AND APPLICATIONS

Proc IMechE Part L:
J Materials: Design and Applications
2022, Vol. 236(3) 633–646

DOI: 10.1177/14644207211053123
journals.sagepub.com/home/pil
SAGE

Machine learning application for evaluating the friction stir processing behavior of dissimilar aluminium alloys joint

Shubham Verma[1], Velaphi Msomi[2], Sipokazi Mabuwa[2], Ali Merdji[3], Joy Prakash Misra[4], Usha Batra[5] and Sandeep Sharma[1]

Abstract

This paper reports on the employment of the machine learning (ML) techniques, namely support vector machine (SVM), artificial neural networks (ANN), and random forest (RF), for predicting the tensile behavior of friction stir processed (FSP) dissimilar aluminium alloys joints (6083-T651 and 8011-H14). The dissimilar aluminium joints are fabricated using the friction stir welding (FSW) process. After that, the friction-stir welded joints are subjected to the FSP procedure at different combinations of process parameters. The rotational speed, traverse speed, and tilt angle are used as the input parameters, while tensile strength and grain size are used as the output parameters. In addition, three performance characteristics (i.e., coefficient of correlation (CC), mean absolute error (MAE), and root mean square error (RMSE)) are used to check the adequacy of the developed model of ML techniques. It is observed that support vector machine_radial basis function kernel is the most accurate modeling technique for predicting the tensile behavior of processes samples. Furthermore, the optical microscope is also utilized to check the grain size of the nugget zone (NZ) of the weld bead for FSP. It is found that the minimum grain size (i.e., 5.06 μm) is obtained for the FSP sample and this grain size corresponded to the high ultimate tensile strength (UTS). Moreover, the fractographic analysis showed the ductile behavior of FSW and FSP samples.

Keywords

Friction stir welding, friction stir processing, dissimilar aluminium alloys, machine learning techniques, ultimate tensile strength, and grain size

1. Introduction

Friction stir processing (FSP) is a microstructural modifying technique that is derived from the friction stir welding (FSW) process.[1–3] Earlier, it was used on a single plate without any material addition. Nowadays, it is utilized to produce hybrid surface composites with improved properties by adding nanoparticles.[4–9] It is also utilized for improving the properties of welded joints. Several studies are carried out to find out the optimal process parameters for FSP/FSW using various techniques such as the Taguchi technique, response surface methodology (RSM), etc.[10,11] Mallieswaran et al.[10] employed RSM for designing the number of experiments for the FSW process. It is observed that the developed regression model is capable of giving the optimal values of process parameters. Butola et al.[11] employed the friction stir process technique (FSP) for the fabrication of surface composites of AA7075 matrix. In this work, Taguchi method is employed for designing the number of experiments at different process parameters. It is found that the rotational tool speed is the most significant factor, followed by reinforcement types and tool geometry. In addition, several researchers utilized the machine learning approached for validating the experimental results.[12,13] Hussain et al.[12] used a machine learning approach (i.e., artificial neural network

[1]Mechanical Engineering Department, Maharishi Markendeshwar (Deemed to be) University Mullana, Haryana, India
[2]Faculty of Engineering and the Built Environment, Cape Peninsula University of Technology, Bellville, South Africa
[3]Faculty of Engineering and Technology, Mascara University, Mascara, Algeria
[4]Mechanical Engineering Department, IIT BHU Varanasi India, Varanasi, Uttar Pradesh, India
[5]School of Engineering, GD Goenka University, Gurugram, India

Corresponding author:
Shubham Verma, Mechanical Engineering Department, Maharishi Markendeshwar (Deemed to be) University Mullana, Haryana, India.
Email: shubham6140005@gmail.com

(ANN)) for predicting the values of energy consumption during the FSP process. It is observed that the ANN technique is capable of predicting the values of performance characteristics. Recently, Verma et al.[13] used different machine learning approaches in order to predict and validate the experimental results on the FSW process of AA7039. It is concluded that the ANN technique is most suitable for predicting the values of process parameters for AA7039.

According to the best knowledge of the authors, maximum work is carried out to study the various properties of the FSP/FSW technique at different process parameters for similar materials. Hence, the previous research work lacks the investigation of machine learning approaches for the FSP technique. Moreover, it is also witnessed that no significant research work is available on the FSP of friction stir welded joints. In the present research work, aluminium alloys 6083-T651 and 8011-H14 are joined by the FSW technique to form a dissimilar joint. The friction stir welded dissimilar joints are then subjected to the FSP procedure using different process parameters. Generally, the FSP technique is employed on the FSW joint to reduce or eliminate some defects resulting from welding more especially when joining materials with distinct mechanical and thermal properties.

Furthermore, machine learning (ML) approaches such as support vector machine (SVM), artificial neural network (ANN), and random forest (RF) techniques are utilized to predict and validate the FSP experimental results on a welded sample of dissimilar aluminium alloys. The software Weka 3.9.4 is used for employing the machine learning approaches. The experimentation is carried at different rotational speeds (rpm), transverse speeds (mm/min), and tilt angles (degree) for obtaining the necessary data sets to train the approaches. Moreover, for predicting the values of performance parameters using the SVM technique, three different kernels, viz. poly kernel (PK), Pearson VII (PUK), and radial based kernel function (RBF) are utilized. The capabilities of ML approaches are evaluated by graphs for train data sets. In the end, the results of all the ML techniques are compared to find out the best technique for predicting and analyzing the present study results. Furthermore, microstructural and fractographical analyses are also carried out for a better understanding of the process.

Table 1. Processing parameters and their levels.

Symbol	Input Parameter	Level Low	Level High	Units
RS	Rotational Speed	400	1300	rpm
TS	Transverse Speed	40	100	mm/min
TA	Tilt Angle	1	3	degrees
PG	Triangular Pin Geometry			

2. Experimental procedure

In current research work, 6 mm thick plates of AA6083-T651 and AA8011-H14 (AA6083/AA8011) are dimensioned into 250 x 50 mm as per the requirement of the fixture of FSW machine (*Make: LAGUN FA.1-LA semi-automatic machine*). The experimentation is carried out in two phases: In the 1st phase, the two dissimilar aluminium alloys are joined by the FSW process to produce a set of 72 plates of dissimilar joints. The joints are fabricated at a rotational speed of 1200 rpm, the traverse speed of 50 mm/min, and the tilt angle of 2^{o} using FSW machine. The welded dissimilar joints are subjected to friction stir processing (FSP) at different rotational speed (RS), transverse speed (TS), and tilt angle (TA) for the 2nd phase of the study. The plates are utilized in this study have a chemical composition similar to the ones reported in the literature.[14] The process parameters for the FSP technique is depicted in Table 1. Table 2 depicts the process parameter combinations used for the current research work. The triangular tool pin profile

Table 2. Experimental outcomes for FSP experiments.

S.No.	RS (rpm)	TS (mm/min)	TA (°)
1	400	40	1
2	400	40	2
3	400	40	3
4	400	60	1
5	400	60	2
6	400	60	3
7	400	100	1
8	400	100	2
9	400	100	3
10	700	40	1
11	700	40	2
12	700	40	3
13	700	60	1
14	700	60	2
15	700	60	3
16	700	100	1
17	700	100	2
18	700	100	3
19	1000	40	1
20	1000	40	2
21	1000	40	3
22	1000	60	1
23	1000	60	2
24	1000	60	3
25	1000	100	1
26	1000	100	2
27	1000	100	3
28	1300	40	1
29	1300	40	2
30	1300	40	3
31	1300	60	1
32	1300	60	2
33	1300	60	3
34	1300	100	1
35	1300	100	2
36	1300	100	3

used in conducting FSW and FSP is made up of HSS (AISI4140) with a shoulder diameter of 20 mm, a pin length of 5.8 mm, and a pin diameter of 7 mm.[9] The experiments are replicated twice in order to raise the level of accuracy. Moreover, during the experimentation AA6083 plate is kept on the advancing side (AS), whereas the AA8011 plate is placed on the retreating side (RS). The experimental setup for the FSP process is illustrated in Figure 1. The tensile specimens are fabricated according to the ASTM-E8M-04 standard. The tensile testing is conducting on Hounsfield tensile testing machine. The strain rate of 2 mm/min is used for conducting all tensile tests under room temperature environment. Afterward, the specimens for microstructural analysis are prepared and then chemically etched with Keller's etchant for AA8011 and Weck's etchant for AA6082. The optical microscope (*Make: Motic AE2000Met inverted microscopy*) is utilized to check the macrostructure of the welded specimens. In addition, the linear intercept technique (ImageJ software) is employed to measure the grain size at the stir zone of the joint. The fractured surfaces after the tensile testing are analyzed by using scanning electron microscopy (SEM).

3. Modelling Using ML (SVM, ANN, and RF)

In this research work, SVM, ANN, and RF are utilized for developing the regression models for a better understanding of the FSP process. The performance parameters for the current study are ultimate tensile strength (UTS) and grain size. In the first step, the experimental data is segregated into the ratio of 3:1, i.e., 75% for the training data set and 25% for the testing data set. Subsequently, training data set is used to develop the regression model. In contrast, the testing data set is used to check for the suitability of the developed model. Furthermore, coefficient of correlation (CC), root mean squared error (RMSE) and mean absolute error (MAE) are considered as performance parameters for developed regression models.

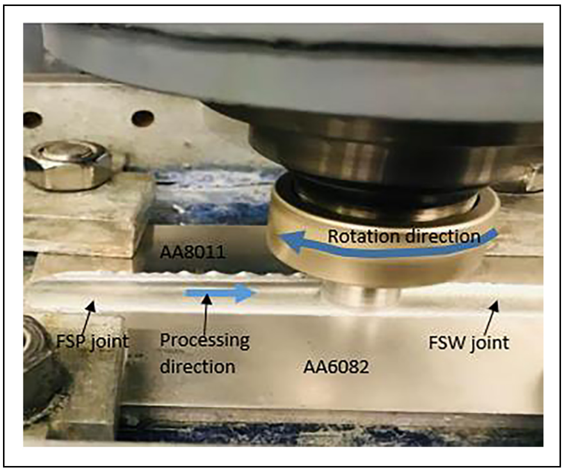

Figure 1. Experimental setup of friction stir processing.

3.1 Support vector machining

SVM is a machine-learning process utilized for the classification problem. However, the SVM method can also be useful to the regression problems.[15,16] The classification in SVM is done by drawing a hyperplane that splits the data points into distinct classes. There may be numerous line segments/planes that separate the data points. But the main purpose is to find a line segment for which the perpendicular distance between the line segment and the extreme points is maximum. The line segment for which the segregation among the classes is maximum is called a hyperplane (see Figure 2). The extreme data points of the classes are termed the support vectors. The equation for an n-dimensional linear hyperplane is presented in Equation 1.

$$\beta_0 + \beta_1 x_1 + \beta_2 x_2 + \ldots + \beta_n x_n = 0 \tag{1}$$

The position of the data point in the hyperplane can be classified into n-1 categories. In 2-D space, 'y' is classified as positive or negative, as given by Equation 2 and Equation 3, respectively.

$$\beta_0 + \beta_1 x_1 + \beta_2 x_2 > 0 \tag{2}$$

$$\beta_0 + \beta_1 x_1 + \beta_2 x_2 < 0 \tag{3}$$

3.2 Artificial neural network

For complicated non-linear problems, the ANN computing tool is used.[17] ANN consists of a large number of interconnected elements. The elements are interconnected by using the weight connections. The networks can perform a definitive function.[18] Figure 3 presents the ANN tool configuration. The networks are configured in a way that each input leads to a definitive output. This

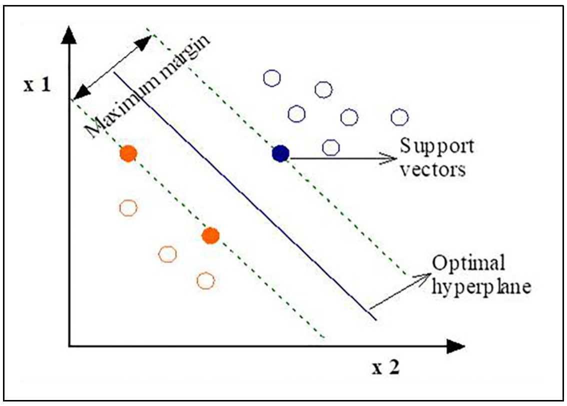

Figure 2. Hyperplane as obtained in SVM, which divides data points into classes.[11]

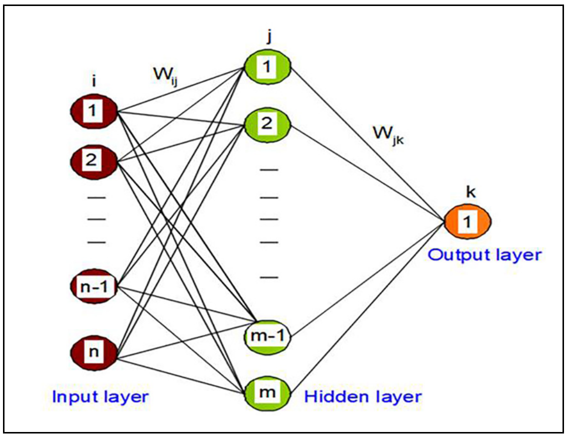

Figure 3. Architecture of ANN.[13]

process is carried out till the difference between the sum of squares of the actual and predicted value is minimized. Numerous researchers designed a large number of ANN networks.[19] The hit and trial method are used to monitor user-defined parameters like learning rate, momentum, and hidden layer. The user-defined parameters are based on the maximization of the root mean square error and coefficient of correlation.

3.3 Random forest regression

In this technique, the number of tree predictors is combined to form a forest for accurately obtaining and predicting the values. The trees are developed independently from their input vectors. The solution for both regression problem and classification problem can be achieved by this method. In place of finding the solution by splitting the node, this approach provides an optimal solution among a number of sub-solutions. In comparison to the other machine learning approaches, the random forest regression method provides higher randomness to the model. The process develops a large variety which leads to a superior model. For the growth of the tree, the variables are randomly selected at each node. The random forest method works on the principle of bringing together a number of binary decision trees generated from the number of bootstraps samples. The samples output of the learning set 'L' is selected randomly at the node, a subset of predictor values X. Further, Breiman et al.[20] used a CART model for the growth of the tree with pruning one or without pruning. In addition to the CART model, Breiman.[26] also used the random forest method. A number of other researchers have reported different ways of selecting variables for the initiation of the tree.[20–22] These procedures are a direct measure of the quality of the variables. The most common approach for selecting a variable for the tree initiation is Information Gain Ratio (IGRC) and Gini Index (GI). In this research, GI is utilized for variable selection. The impurities of a variable can be accessed by GI and are in connection with the output. In the specific model, a full-grown tree is used. The tree is not trimmed as compared to the M5P tree method. Trees are growing up to a maximum depth of new training data.[22] This machine learning can obtain a high number of outputs from a singular input. For the prediction free zone, it uses average output that improves the reliability of the approach.[23] In the current research, m and k is used as the user-defined parameters of a random forest regression. In the present investigation, m presents the number of variables at every node of the tree, whereas k presents the number of trees to be grown.

Table 3. Parameters of ML.

Classifiers	User-defined parameters
SVM_PK	C=1, E = 12
SVM_PUK	C=3, ω= 1, σ = 1.5
SVM_RBF	C=1, γ= 0.3
ANN	Learning rate = 0.4, momentum = 0.3, Iteration =500, Hidden layer = 4
RF	K = 1, m = 1, I = 1000

3.4 Kernels for SVM

The kernel in SVM maps the non-linear function at the input to a linear function in the feature space. SVM uses kernels to get the output. Based upon the performance criteria, radial basis function (RBF) and PUK kernels have been proposed.[24,25] Linear kernels work on the datasets that are separated linearly, while the non-linear kernels are used for non-linearly separated datasets. As per the requirement, different kernels are used for different requirements of finding the optimized hyperplane. Equation (4) presents the polynomial kernel functions.[25].

$$K(x_1, x_2) = ({x_1}^T x_2 + 1)^p \tag{4}$$

Equation 5 presents the generalized function for the polynomial kernel, and Equation 6 presents the corresponding constraints.

$$Q(\alpha) = \sum_{i=1}^{N} \alpha_i - \frac{1}{2}\sum_{i=1}^{N}\sum_{j=1}^{N} \alpha_i \alpha_j d_i d_j K(x, x_i) \tag{5}$$

$$\sum_{i=1}^{N} \alpha_i d_i \tag{6}$$

Equations (7) and (8) presents the RBF and PUK kernels below.[25].

$$\text{RBF Kernel}(e{-}^{\gamma}|x_i - x_j|^2) \tag{7}$$

$$\text{Pearson VII function Kernel} \times \left(\frac{1}{\left[1 + \left(2\sqrt{x_i - x_j}^2 \sqrt{2^{\left(\frac{1}{\omega}\right)} - 1} \,/\, \sigma\right)^2\right]^{\omega}} \right) \tag{8}$$

Where kernel specified parameters are designated as γ, σ, and ω. In the PUK kernel, σ represents the Pearson width,

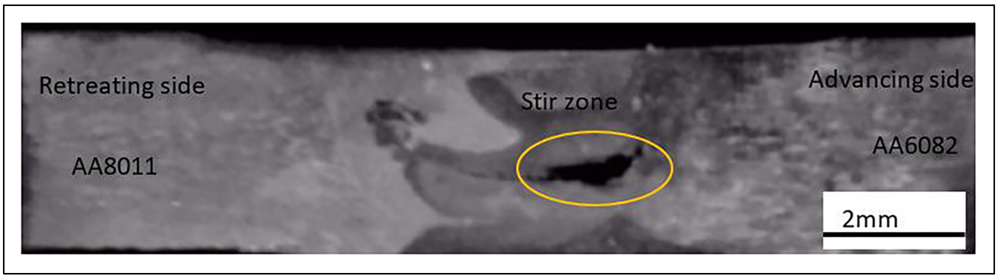

Figure 4. Macrostructure of friction stir welded joint (higher strength specimen).

and ω represents the trailing factor of the peak value. SVM technique applies kernels to establish an optimized user-defined parameter. The accuracy of the technique depends upon the parameter effectiveness. The requirement of SVM is to determine the regularization parameter 'C' and error-insensitive zone size 'ϵ'. On the contrary, Gaussian noise levels are required for GPR. Hit and trial is employed to get optimum values of parameters like C, γ, σ, ω, and Gaussian noise for SVM. For the best model, minimum RMSE, MAE, and maximum CC is considered. Table 3 presents the optimized parameters. Polynomial Kernel, Pearson VII kernel, and radial basis kernel functions for SVM are denoted as SVM_PK, SVM_PUK, and SVM_RBF, respectively.

3.5 Data set selection

The user-defined parameters played an important role in the implementation of ML techniques. These parameters checked the competency of developed regression models. User-defined parameters are chosen on the basis of CC and RMSE values. The obtained parameters maximum values of CC and RMSE are selected on the basis of the hit and trial method. Firstly, user-defined parameters for the training data set are selected. Afterward, the same parameters testing data set is trained to develop a regression model.[13] The user-defined parameters are presented in Table 3.

4. Results and Discussion

4.1 FSW results (tensile and macrostructural analysis)

In the first phase, FSW experiments are carried out as per Table 2. The maximum UTS is obtained for parent metals (i.e., 303 MPa for AA6082 and 103 MPa for AA8011). The maximum value of UTS (i.e., 39.83 MPa) for FSW is obtained at a rotational speed of 1000 rpm, a transverse speed of 40 mm/min, and a tilt angle of 1°. The joint strength is found to be lower than the parent metals. It is attributed to the strengthening mechanism of second phase particles. Moreover, it is also due to the placement of higher strength material AA6082 on the AS.[9, 27]

Figure 4 illustrates the macrostructure of the friction stir welded joint (higher strength specimen, i.e., 39.83 MPa). It is evident that minor defects in the form of small holes are observed at the NZ. It is owing to the poor material bonding between dissimilar aluminium alloys.

Table 4. Experimental outcomes for FSP process.

RUN	RS (rpm)	TS (mm/min)	TA (°)	UTS (MPa)	Grain Size
1	400	40	1	35.32	23.12
2	400	40	2	30.41	21.37
3	400	40	3	41.53	20.61
4	400	60	1	26.81	21.83
5	400	60	2	33.74	22.58
6	400	60	3	27.25	24.92
7	400	100	1	28.37	22.06
8	400	60	2	31.58	20.87
9	400	100	3	37.08	21.03
10	700	40	1	43.27	16.59
11	700	40	2	40.51	16.88
12	700	40	3	37.97	13.61
13	700	60	1	47.33	12.96
14	700	60	2	67.39	10.08
15	700	60	3	63.83	11.64
16	700	100	1	78.30	9.68
17	700	100	2	81.36	9.24
18	700	100	3	81.09	9.98
19	1000	40	1	83.61	8.41
20	1000	40	2	89.48	7.83
21	1000	40	3	88.07	8.06
22	1000	60	1	74.38	6.85
23	1000	60	2	76.33	6.97
24	1000	60	3	71.06	7.56
25	1000	100	1	69.34	7.06
26	1000	100	2	70.18	6.81
27	1000	100	3	73.54	7.08
28	1300	40	1	89.32	6.53
29	1300	40	2	91.68	5.86
30	1300	40	3	90.22	5.98
31	1300	60	1	88.96	5.07
32	**1300**	**60**	**2**	**92.94**	**5.06**
33	1300	60	3	91.87	6.07
34	1300	100	1	78.39	6.43
35	1300	100	2	81.34	5.11
36	1300	100	3	76.73	5.36

4.2 FSP results (tensile and macrostructural analysis)

Table 4 represents the experimental outcomes for the FSP technique. Maximum UTS (i.e., 92.94 MPa) is obtained

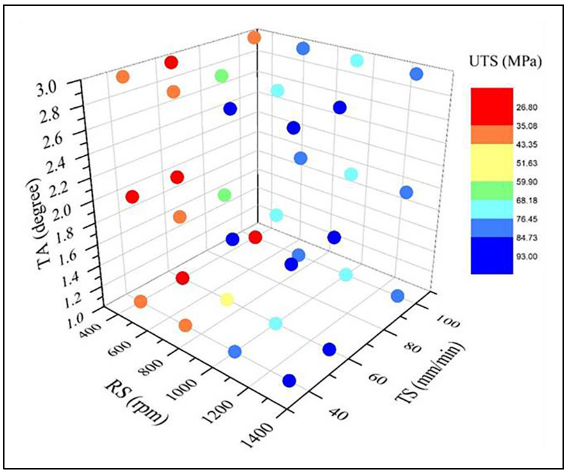

Figure 5. 3D plots between UTS and input parameters.

for run 32. Figure 5 illustrates the 3D plots between the UTS and the process parameters. Maximum UTS is obtained in a region where rotational speed is moderate and varies from 1000–1300 rpm, tilt angle varies between 2^{o}–3^{o}, and transverse speed varies between 40–60 mm/min. It is owing to proper heat generation between the tool and the workpiece. Another reason is the proper mixing of material at the nugget zone during the processing process. It is also visible from Figure 5, the minimum values of UTS are obtained where the minimum rotational speed, maximum weld steed, and the maximum tilt angle are used. It is attributed to improper heat generation during the process.

Figure 6 shows the macrostructure of AA6082/AA8011 dissimilar joints that are subjected to the FSP process (i.e., run 3, run 17, run 20, and run 32). The specimens that are processed using low rotational speed indicated poor materials mixing and visibility of large size defects at the stir zone, as shown in Figure 6 (a) and Figure (b). In contrast, Figure 6 (c) and Figure (d) showed defect-less joints after the FSP process. It is owing to proper heat generation at higher rotational speed and results in appropriate mixing of material at NZ.

Figure 6 illustrates the 3D plots between the UTS and the process parameters. Maximum UTS is obtained in a region where rotational speed is moderate and varies from 1000 to1300 rpm, and tilt angle varies between 2^{o} to $3^{o,}$ and transverse speed ranges between 40 to 60 mm/min. This behavior was attributed to the proper heat generation between the tool and the workpiece, which then resulted in the proper mixing of material at the nugget zone during the FSP procedure. It is also visible

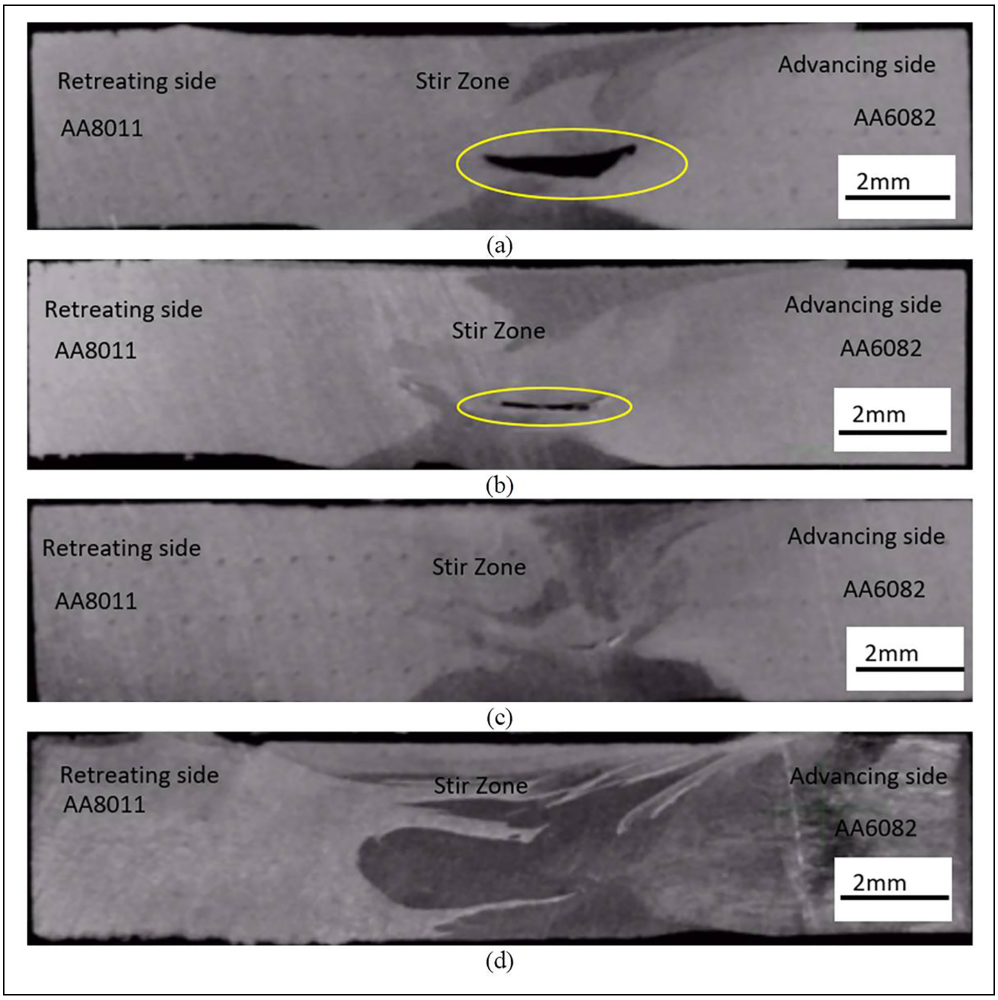

Figure 6. Macrograph of (a) run 3, (b) run 17 (c) run 20 and (d) run 32.

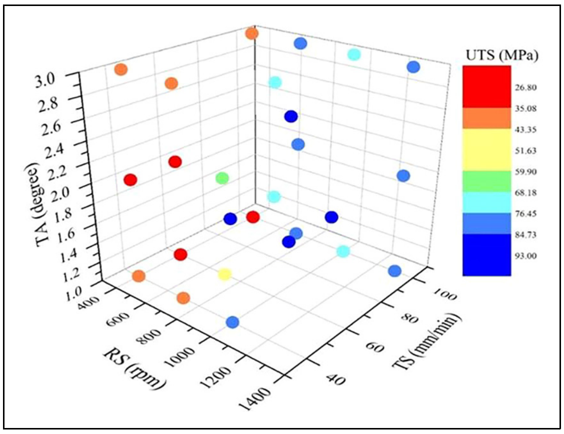

Figure 7. 3D plot for the training data set.

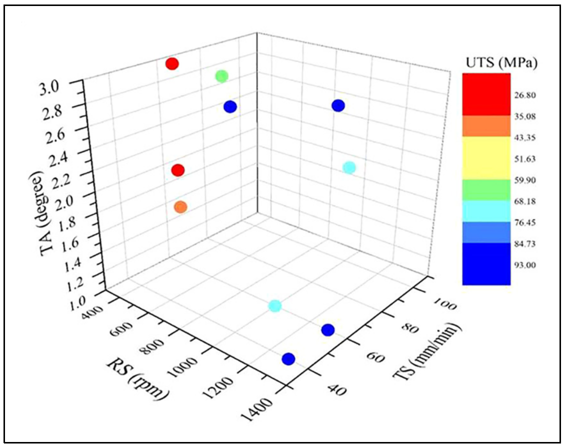

Figure 8. 3D plot for the testing data set.

from Figure 6 that the minimum values of UTS were obtained where the minimum rotational speed, maximum weld speed, and maximum tilt angle were used. This behavior was attributed to improper heat generation during the process.

Figure 6: 3D plots between UTS and input parameters

4.3 ML regression model analysis

The 3D plots for the training data set and testing data set are shown in Figure 7 and Figure 8. The maximum values of UTS are observed in the region where rotational speed, transverse speed, and tilt angle varied between moderate to maximum values.

Primarily, training data is trained in Weka Software at various values of user-defined parameters up to optimal values of user-defined parameters (i.e., CC). After getting the optimal values of user-defined parameters, the predicted values of UTS are recorded, as shown in Table 5. Afterward, the testing data is trained to obtain the predicted UTS values at the same optimal values of user-defined parameters, as depicted in Table 6. Moreover, graphical analysis is also carried between the actual values and predicted values of ML approaches in order to check the adequacy of the developed model for

Table 5. Actual and predicted values of ML techniques (training data set).

S. No.	RS	WS	TA	Actual (UTS)MPa	SVM (UTS(MPa)) PK	PUK	RBF	ANN UTS (MPa)	RF UTS (MPa)
1	400	40	1	35.32	35.04	35.30	25.03	34.14	35.25
2	400	40	2	30.41	37.71	30.41	31.51	34.29	34.31
3	400	40	3	41.53	40.37	41.47	39.38	34.31	39.73
4	400	60	1	26.81	35.84	26.68	26.82	29.00	30.00
5	400	60	2	33.74	38.50	33.87	33.79	34.31	35.46
6	400	100	1	28.37	32.91	28.48	33.50	37.40	33.82
7	400	100	3	37.08	37.11	37.09	45.17	39.54	40.15
8	700	40	1	43.27	53.77	43.72	46.92	48.08	45.80
9	700	40	3	37.97	57.97	37.99	57.89	42.33	46.12
10	700	60	1	47.33	53.44	47.42	48.38	52.24	52.42
11	700	60	2	67.39	56.11	65.43	55.55	62.47	66.54
12	700	100	1	78.3	50.51	62.80	51.98	73.99	73.26
13	700	100	2	81.36	53.18	81.29	58.06	79.63	79.09
14	700	100	3	81.09	55.84	74.03	61.45	78.56	77.59
15	1000	40	1	83.61	72.51	83.48	70.29	81.71	79.72
16	1000	40	2	89.48	75.17	86.08	76.86	91.58	86.47
17	1000	60	2	76.33	73.71	86.19	76.33	78.58	78.19
18	1000	60	3	71.06	76.37	71.07	77.49	75.60	73.59
19	1000	100	1	69.34	69.24	69.45	69.30	69.80	71.08
20	1000	100	3	73.54	73.44	73.61	73.43	80.07	73.99
21	1300	40	2	91.68	91.64	91.74	91.67	100.54	89.96
22	1300	40	3	90.22	94.31	90.09	90.10	89.83	86.06
23	1300	60	2	92.94	91.31	92.88	90.36	93.09	88.33
24	1300	100	1	78.39	85.71	78.35	78.44	74.65	77.40
25	1300	100	2	81.34	88.38	81.46	81.46	82.57	81.31
26	1300	100	3	76.73	91.04	76.63	78.91	81.65	78.06

Table 6. Actual and Predicted values of UTS for ML techniques (testing data set).

S. No.	RS	WS	TA	Actual (UTS)MPa	SVM (UTS(MPa)) PK	PUK	RBF	ANN UTS (MPa)	RF UTS (MPa)
1	400	60	2	31.58	48.12	53.24	44.98	36.61	49.89
2	700	40	2	40.51	61.53	68.87	60.05	63.93	63.13
3	1000	40	3	88.07	73.88	62.18	74.78	77.11	71.97
4	1300	40	1	89.32	81.62	86.73	79.83	88.91	71.26
5	1300	60	3	91.87	82.10	75.60	81.56	78.94	72.46
6	400	60	3	27.25	49.65	48.65	50.10	38.83	51.19
7	700	60	3	63.83	60.47	55.22	62.05	71.32	62.31
8	1000	60	1	74.38	68.21	71.47	66.91	84.89	65.31
9	1000	100	2	70.18	64.56	79.56	68.62	82.78	71.61
10	1300	60	1	88.96	79.03	80.39	77.88	94.71	68.37

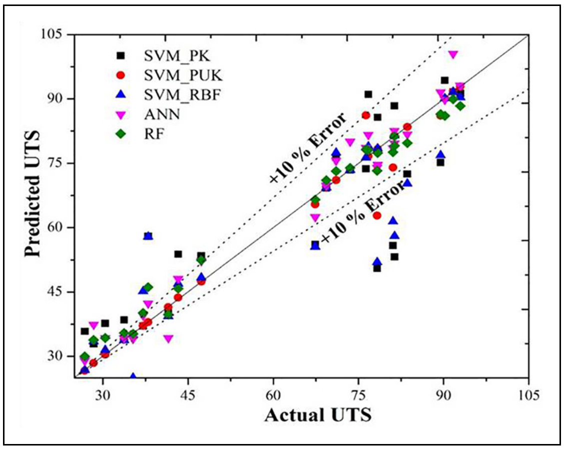

Figure 9. Training data set (Actual Vs. Predicted values).

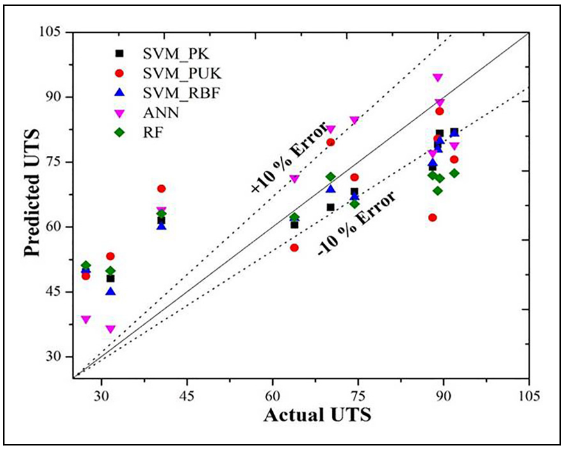

Figure 10. Testing data set (Actual vs. Predicted).

training and testing data sets. Figure 9 and Figure 10 demonstrate the graphical analysis for training and testing data sets. It is evident that the graphs consist of three distinct lines (i.e., one perfect line (at 45°) and two error lines range between $\pm$ 10%). These lines play an important role in the graphical analysis of ML that confirms the adequacy of the developed model. The predicted values

Table 7. Values of CC, RMSE, and MAE.

Machine learning approach	Training data set CC	RMSE UTS(MPa)	MAE UTS (MPa)	Testing data set CC	RMSE UTS (MPa)	MAE UTS (MPa)
SVM_PK	0.848	12.008	8.622	0.946	13.240	8.6227
SVM_PUK	0.985	3.935	1.526	0.731	17.081	14.564
SVM_RBF	0.898	10.312	6.542	0.961	11.637	10.070
ANN	0.983	4.272	3.507	0.905	12.809	11.075
RF	0.993	3.353	2.785	0.908	17.003	15.100

of the training data set for all ML techniques are depicted in Figure 9. The maximum predicted values compared with actual values are obtained in the range of $\pm$ 10% error lines. It is also evident that few values are obtained outside the error lines, whereas some predicted values are obtained at the perfect line. Moreover, it is noted that maximum points are visible at a perfect line that an indication of the adequacy of the training data set. The performance parameters (i.e., CC, RMSE, and MAE) are utilized to verify the suitability of the developed model.

For the present research work, the performance parameters of ML techniques are depicted in Table 7 for both data sets. The maximum and minimum values of CC for the training data set are observed for RF and SVM_PUK. Conversely, the maximum and minimum error is obtained for SVM_PUK and RF. The graphical analysis of the testing data set is depicted in Figure 10. The features are similar to the training data set. The maximum points are observed in close proximity of the perfect line is an indication of the adequacy of the developed model. Figure 11 and Figure 12 illustrates the values of performance parameters for both data set. The maximum and minimum values of performance parameters are visible in Figure 11 and Figure 12. These values are used for analyzing the results of ML techniques.

Furthermore, another graphical analysis (between UTS and data sets) is also carried out to observe the adequacy of the developed model for both data sets. Figure 13 and

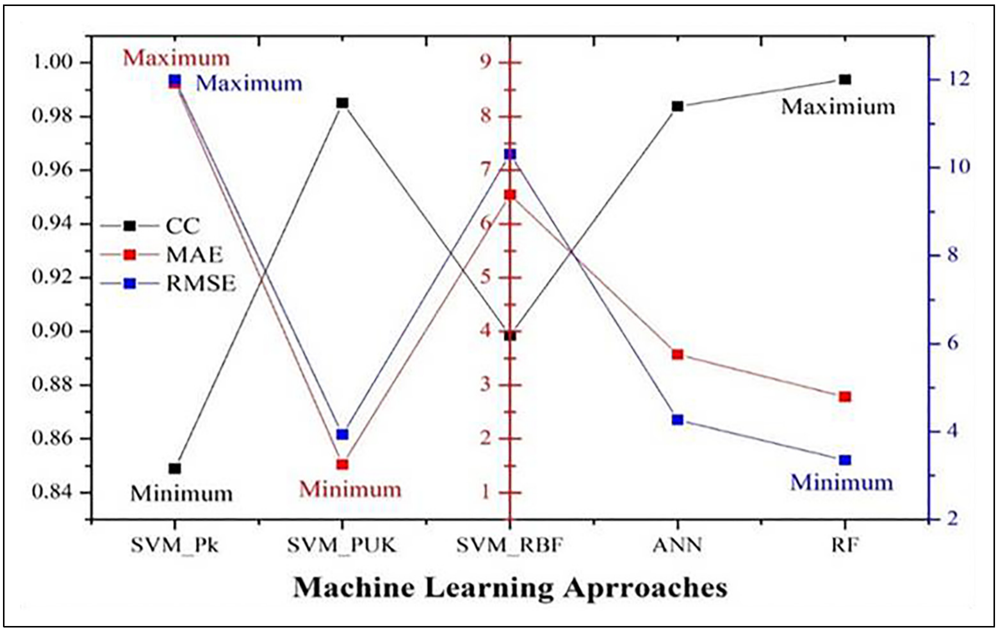

Figure 11. Performance parameters (training data set).

Figure 14 show the representation of UTS and both data sets (training data set and testing data set). It is evident that the predicted values follow a similar path as that of actual values with minimum deviation for all ML techniques for the training data set. The lines of SVM_PUK, SVM_RBF, and RF are observed almost close to the actual line of UTS, as shown in Figure 13. Contrariwise, the lines of ML techniques are almost followed the same as that of the actual values, as shown in Figure 14.

Moreover, the suitability of SVM, ANN, and RF is also checked out by residuals (difference between actual and predicted values) analysis as presented in Figure 15. It is noted that the residual errors are minimum for the SVM_RBF technique as compared to SVM_PK, SVM_PUK, ANN, and RF. It indicates that the SVM_RBF is the most optimal ML approach for current research work.

5 Microstructural Analysis

5.1 FSW sample microstructure

In the current research, microstructural analysis is carried on FSW and FSP samples to determine the grain size of

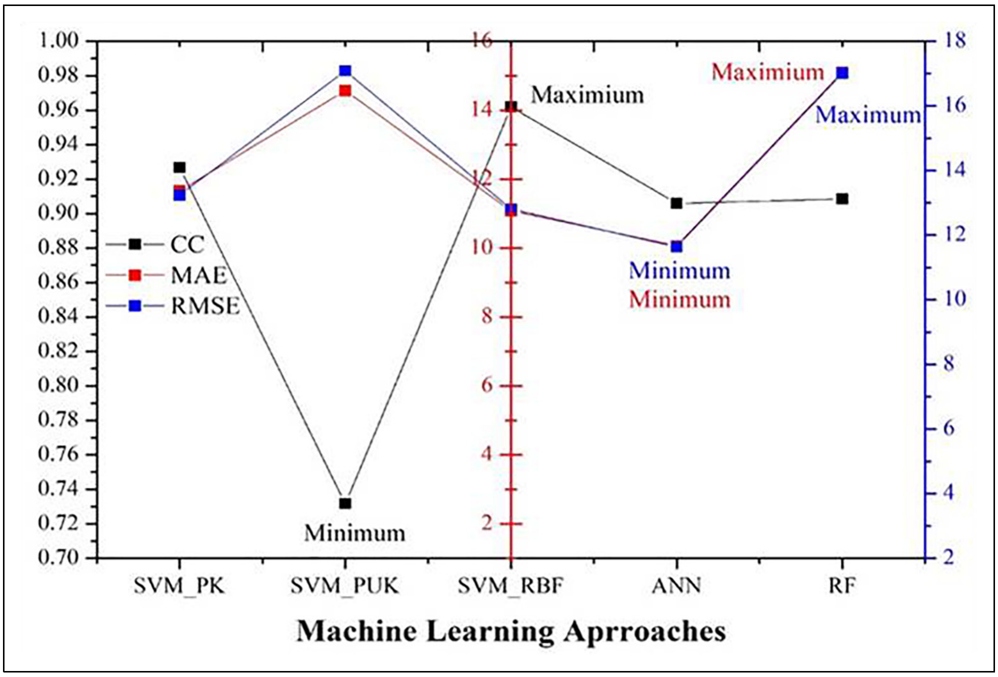

Figure 12. Performance parameters (training data set).

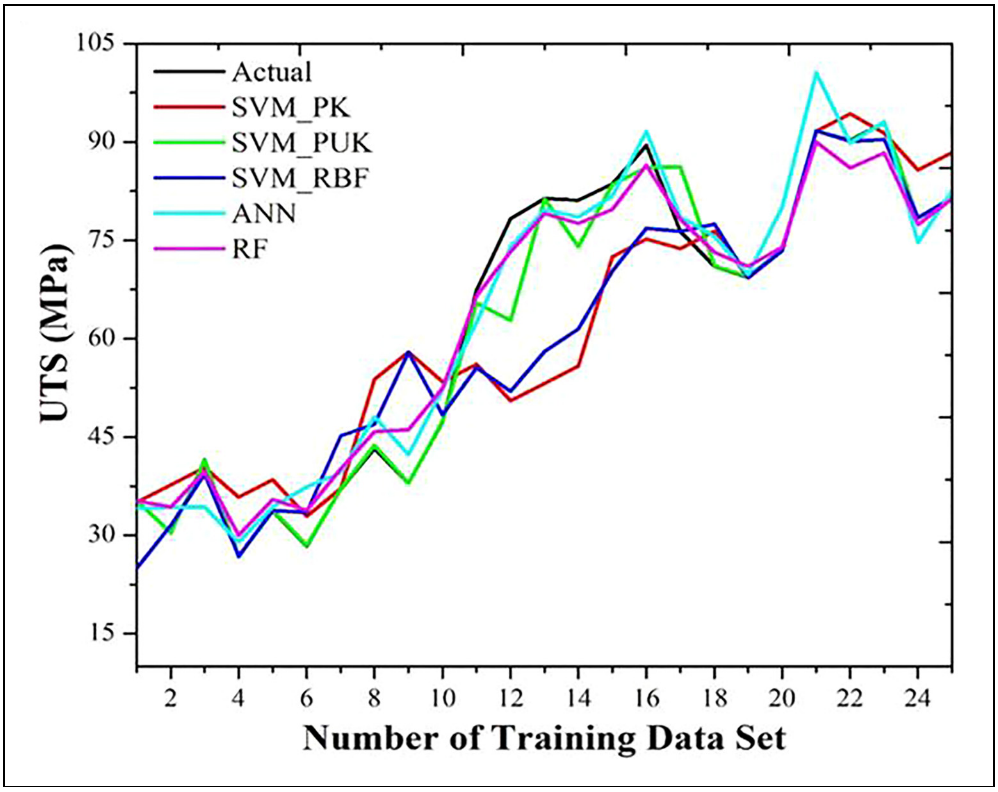

Figure 13. Actual UTS vs. training data set.

the stir/nugget zone. Figure 16 shows the microstructure for the FSW specimen (higher strength specimen) that is used in measuring the average grain size through the linear intercept technique. The average grain size of 28.06 μm is measured for the nugget zone for the FSW sample.

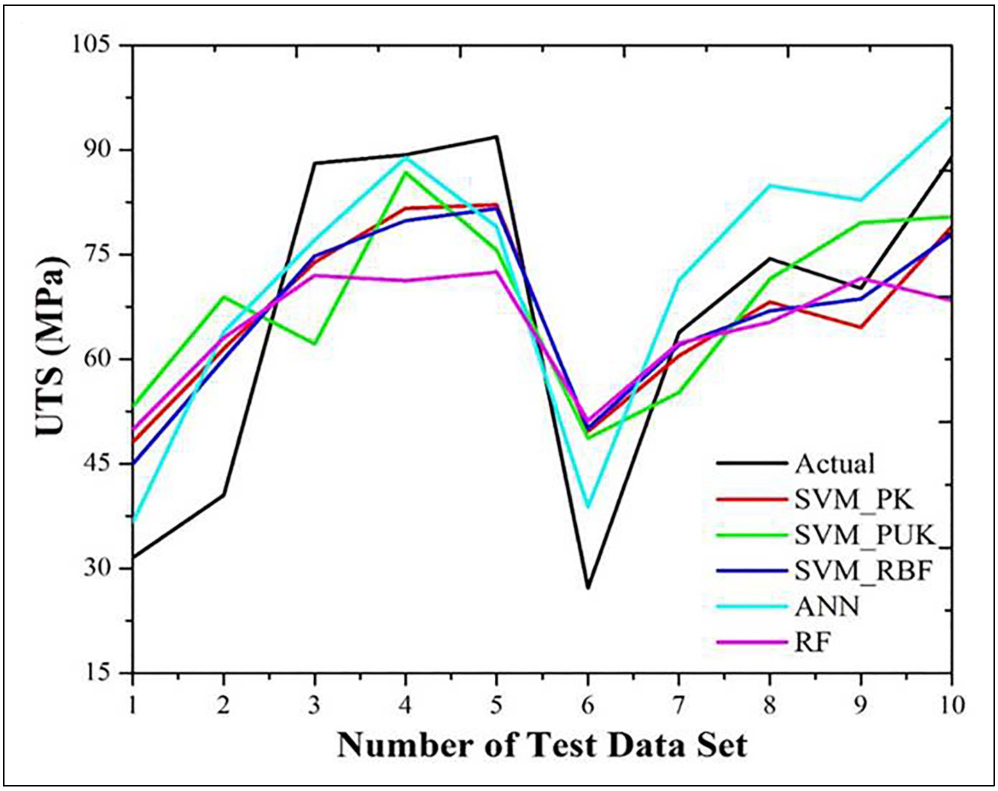

Figure 14. Actual UTS vs. testing data set.

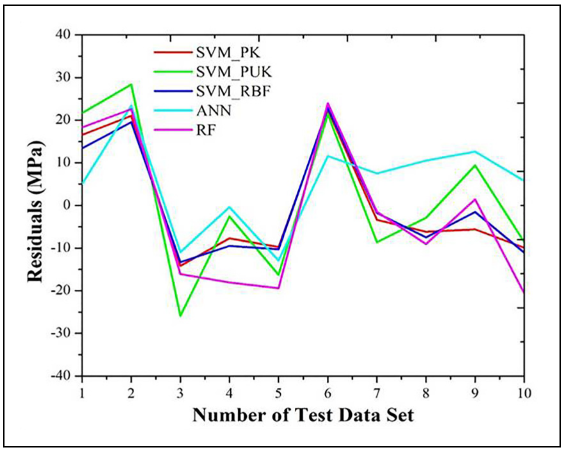

Figure 15. Residuals for testing data sets.

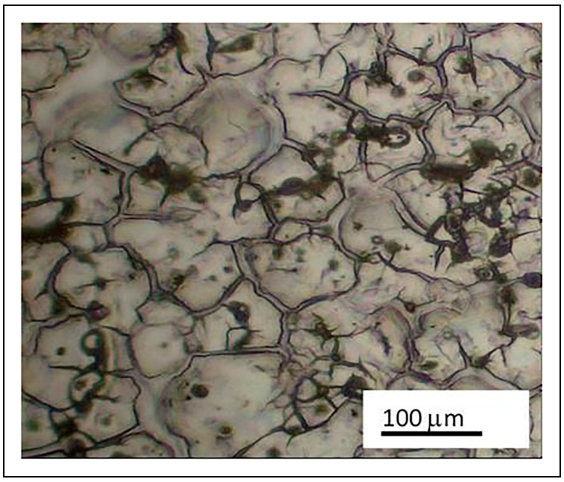

Figure 16. Microstructure of friction stir welded AA6082/AA8011 dissimilar joint sampled at the center of the nugget zone (higher strength specimen).

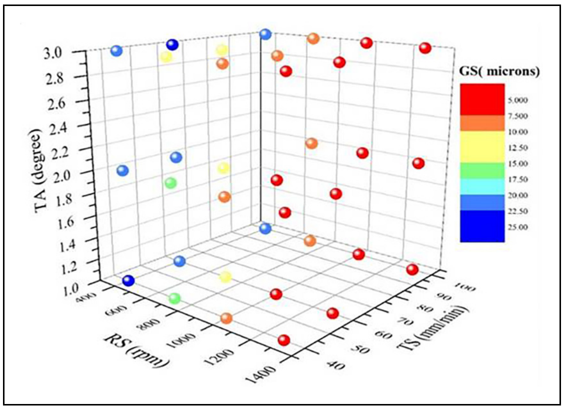

Figure 17. 3D plots for grain size.

5.2 FSP samples microstructures

Figure 17 and Table 4 depict the grain size at different input process parameters. It is observed that minimum grain size is obtained for run 32 (i.e., 5.06 µm, 1300 rpm, 60 mm/min, and 2°). It is evident from Figure 17, the minimum grain size is observed in a region where the rotational speed ranges between 1000 to1400 rpm, transverse speed ranges from 60 to100 mm/min, and a tilt angle range between 1° to 3°. It is attributed towards the proper string phenomena at necessary heat generation. On the other hand, maximum grain size is observed in the region where rotational speed is minimum and transverse speed is maximum. It is happened due to improper stirring phenomena at low heat input.[26]

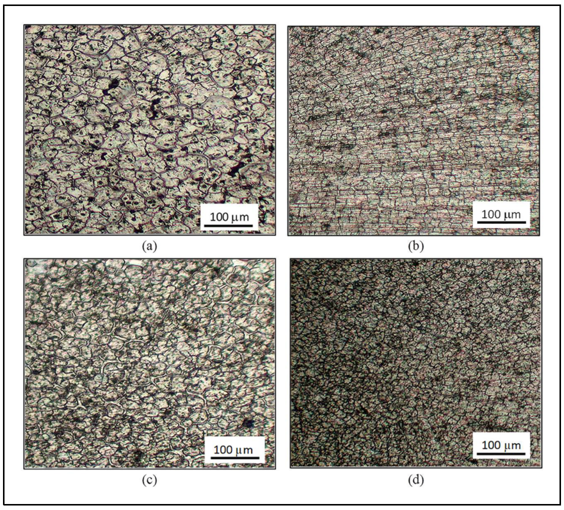

Figure 18. Microstructure at the stir zone for FSP parameters: (a) run 3, (b) run 17, (c) run 20, and (d) run 32.

Figure 18 depicts the microstructural images of run 3, run 17, run 20, and run 32. The grain size is reduced as compared to the FSW process. The minimum grain size is obtained for run 32. Figure 18 (a) shows the microstructure of the FSW sample at minimum rotational speed, maximum tilt angle, and moderate feed rate. The grain size for run 32 is measured as 20 µm. It is an indication of improper stirring at the NZ of the FSP sample due to less softening of the material. It is attributed to lower heat input at a minimum rotational speed. Figure 18 (b) depicts the microstructural image of the sample at maximum feed rate and 700 rpm. The grain size is decreased from 20 µm to 9.24 µm. It results in better stirring phenomena, which increases the heat input with an increase in rotational speed. The minimum grain size of 5.05 µm is observed at 1300 rpm, moderate feed rate (i.e., 60 mm/min), and average values of tilt angle (i.e., 2^{o}) as shown in Figure 18 (d).

6. Fracture Analysis

Fractography analysis is carried out for a better understanding of the process. Figure 19 shows the fractography images of FSW sample of higher strength specimen and FSP samples of run 3, run 17, run 20, and run 32. It is evident that all the samples for FSW and FSP joints showed surfaces with dimples of different sizes, which indicates ductile failure. The dimples of FSW sample (Figure 19 (a)) and FSP run 3 are smaller in size and

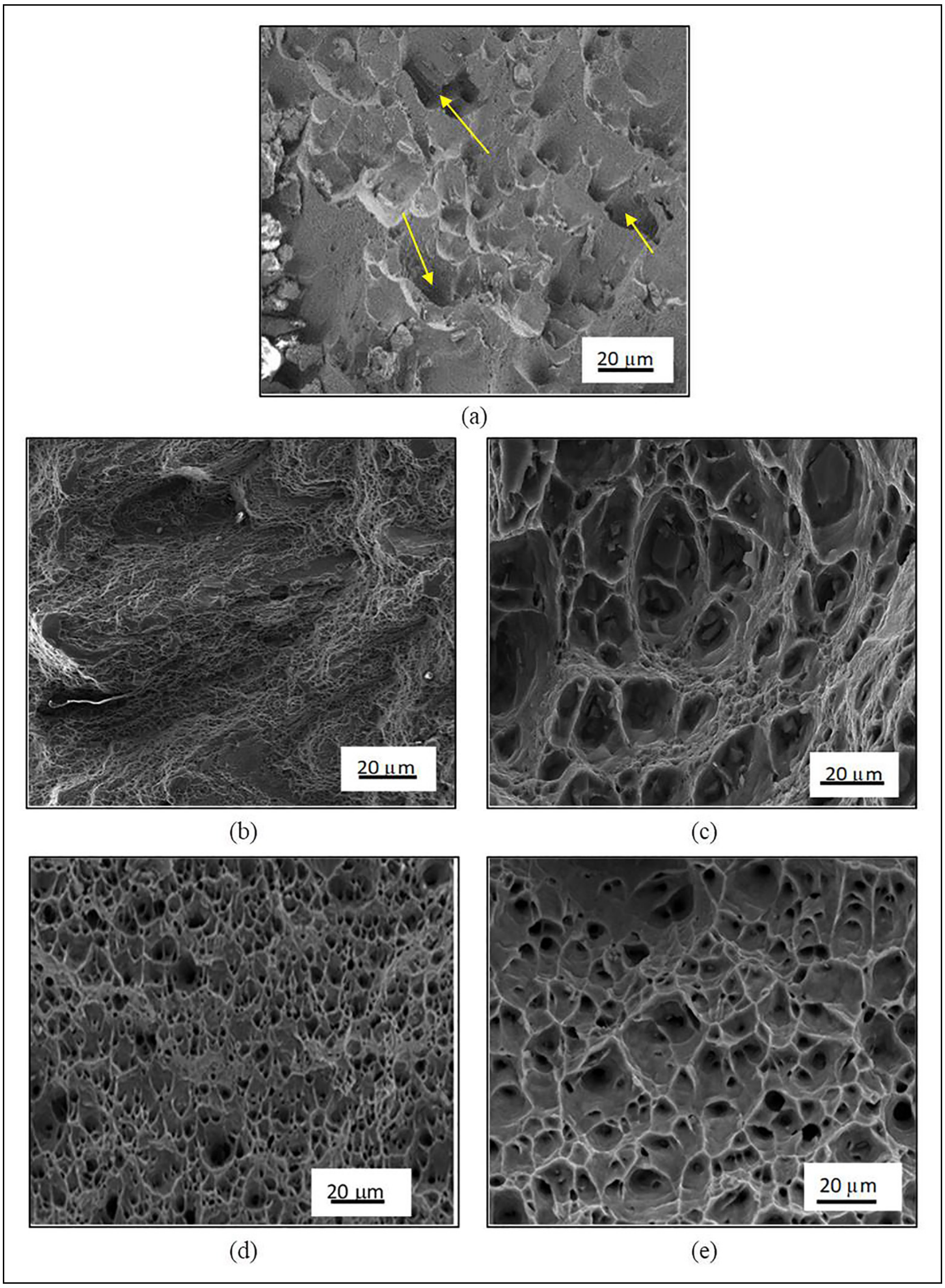

Figure 19. Fractrography images (a) FSW sample of higher strength specimen, (b), (c), (d), and (e) FSP samples of run 3, run 17, run 20, and run 32.

presented the quasi cleavage features owing to less stirring phenomena. In contrast, the larger size and a greater number of dimples are observed on run 17, run 20, and run 32 (Figure 19 (c-e)). Moreover, micro-voids (shown in yellow arrows) are detected on the surface of the FSW specimen. It is occurred due to proper heat generation at the NZ and stirring phenomena.

Conclusions

The present paper reports on the utilization of ML techniques to predict the tensile behavior of friction stir processed FS welded dissimilar aluminium (AA6082-AA8011) joints. The developed regression models of SVM, ANN, and RF are utilized to predict the tensile behavior of processes samples. The findings of the present study are listed below:

- The ML techniques SVM, ANN, and RF are proficient in validating the experimental results of FS processed FS welded joints.
- The maximum CC value for the training data set is obtained for RF, i.e., 0.99 with a minimum value of RMSE, i.e., 3.353.

- SVM_PK regression model for training data set showed the minimum value of CC, i.e., 0.848 with maximum values of RMSE (i.e., 12.008) and MAE (i.e., 8.622).
- The best significant ML technique is obtained by using testing data set. It is concluded that the SVM_RBF is the most significant approach for current research work for predicting the tensile behavior of processed samples with a CC value of 0.961, RMSE value of 11.637, and MAE value of 10.070.
- The graphical analysis is also utilized to validate the different ML techniques results. It concluded that SVM_RBF is the most prominent techniques for current research work.
- The accuracy of different models can be arranged in decreasing order as follows: SVM_RBF, SVM_PK, RF, SVM_PUK, and ANN.
- It is also concluded that the grain size of the higher strength FSW sample is measured as 28.06 μm, whereas for FSP, it is measured as 5.06 μm. It is attributed to the grain refinement phenomena of FSP process.
- The fractography analysis showed the ductile behavior of FSW and FSP samples.

ORCID iD

Shubham Verma https://orcid.org/0000-0002-8417-3333

References

1. Mehrian SM, Rahsepar M, Khodabakhshi F and Gerlich AP. Effects of friction stir processing on the microstructure, mechanical and corrosion behaviors of an aluminum-magnesium alloy. *Surface and Coatings Technology* 2021; 405: 126647.
2. Mabuwa S and Msomi V. Comparative analysis between normal and submerged friction stir processed friction stir welded dissimilar aluminium alloy joints. *Journal of Materials Research and Technology* 2020; 9(5): 9632–44.
3. Ma M, Lai R, Qin J, Wang B, Liu H, Yi D and Zhai T. Achieving exceptionally tensile properties and damage tolerance of 5083 aluminum alloy by friction stir processing assisted by ultrasonic and liquid nitrogen field. *Materials Science and Engineering: A* 2021; 806: 140824.
4. Li J, Li Y, Wang F, Meng X, Wan L, Dong Z and Huang Y. Friction stir processing of high-entropy alloy reinforced aluminum matrix composites for mechanical properties enhancement. *Materials Science and Engineering: A* 2020; 792: 139755.
5. Huang GQ, Yan YF, Wu J, Shen YF and Gerlich AP. Microstructure and mechanical properties of fine-grained aluminum matrix composite reinforced with nitinol shape memory alloy particulates produced by underwater friction stir processing. *Journal of Alloys and Compounds* 2019; 786: 257–71.
6. Kumar H, Prasad R, Kumar P, Tewari SP and Singh JK. Mechanical and tribological characterization of industrial wastes reinforced aluminum alloy composites fabricated via friction stir processing. *Journal of Alloys and Compounds* 2020; 831: 154832.
7. Mabuwa S and Msomi V. Effect of friction stir processing on gas tungsten arc-welded and friction stir-welded 5083-H111 aluminium alloy joints. *Advances in Materials Science and Engineering* 2019; 2019.
8. Msomi V, Mbana N and Mabuwa S. Microstructural analysis of the friction stir welded 1050-H14 and 5083-H111 aluminium alloys. *Materials Today: Proceedings* 2020; 26: 189–92.
9. Mabuwa S and Msomi V. Fatigue behaviour of the multi-pass friction stir processed AA8011-H14 and AA6082-T651 dissimilar joints. *Engineering Failure Analysis* 2020; 118: 104876.
10. Mallieswaran K, Padmanabhan R and Balasubramanian V. Friction stir welding parameters optimization for tailored welded blank sheets of AA1100 with AA6061 dissimilar alloy using response surface methodology. *Advances in Materials and Processing Technologies* 2018; 4(1): 142–57.
11. Butola R, Ranganath MS and Murtaza Q. Fabrication and optimization of AA7075 matrix surface composites using Taguchi technique via friction stir processing (FSP). *Engineering Research Express* 2019; 1(2): 025015.
12. Hussain G, Ranjbar M and Hassanzadeh S. Trade-off among mechanical properties and energy consumption in multi-pass friction stir processing of Al7075 alloy employing neural network–based genetic optimization. *Proceedings of the Institution of Mechanical Engineers, Part B: Journal of Engineering Manufacture* 2017; 231(1): 129–39.
13. Verma S, Misra JP, Singh J, Batra U and Kumar Y. Prediction of tensile behavior of FS welded AA7039 using machine learning. *Materials Today Communications* 2021; 26: 101933.
14. Mabuwa S and Msomi V. The impact of submerged friction stir processing on the friction stir welded dissimilar joints. *Materials Research Express* 2020; 7(9): 096513.
15. Vapnik V. *The nature of statistical learning theory*. Springer science & business media; 2013 Jun 29.
16. Cortes C and Vapnik V. Support-vector networks. *Machine Learning* 1995; 20(3): 273–97.
17. Sebastian S and Puthiyidam JJ. Evaluating students performance by artificial neural network using weka. *International Journal of Computer Applications* 2015; 119(23).
18. Bishop CM. *Neural networks for pattern recognition*. Oxford University Press; 1995 Nov 23.
19. Eberhart RC and Dobbins RW. *Neural Network PC Tools: A Practical Guide*. Academic. San Diego. 1990.
20. Breiman L, Friedman JH, Olshen RA and Stone CJ. Classification and regression trees. Belmont, CA: Wadsworth. *International Group* 1984; 432: 151–66.
21. Breiman L. Bagging predictors. *Machine Learning* 1996; 24(2): 123–40.
22. Verma S, Misra JP and Popli D. Modeling of friction stir welding of aviation grade aluminium alloy using machine learning approaches. *International Journal of Modelling and Simulation* 2020: 1–8.
23. Quinlan JR. Learning with continuous classes. In 5th Australian joint conference on artificial intelligence *1992* Nov 16 (Vol. 92, pp. 343–348).
24. Üstün B, Melssen WJ and Buydens LM. Facilitating the application of support vector regression by using a universal Pearson VII function based kernel. *Chemometrics and Intelligent Laboratory Systems* 2006; 81(1): 29–40.
25. Asraf HM, Nooritawati MT and Rizam MS. A comparative study in kernel-based support vector machine of oil palm

leaves nutrient disease. *Procedia Engineering* 2012; 41: 1353–9.

26. Mabuwa S and Msomi V. The effect of FSP conditions towards microstructure and mechanical properties of the AA6082/AA8011 TIG-welded joint. *Materials Research Express* 2021.

27. Verma S, Gupta M and Misra JP. Effect of pin-profiles on thermal cycle, mechanical and metallurgical properties of friction stir–welded aviation-grade aluminum alloy. Proceedings of the Institution of Mechanical Engineers, *Part B: Journal of Engineering Manufacture* 2019; 233(11): 2183–95.